

## Kinematic and thermodynamic effects on liquid lithium sputtering

J.P. Allain,<sup>1</sup> M.D. Coventry,<sup>2</sup> D.N. Ruzic<sup>2</sup>

<sup>1</sup>*Argonne National Laboratory, Argonne, IL 60439, USA*

<sup>2</sup>*University of Illinois at Urbana-Champaign, Urbana, IL 61801, USA*

### ABSTRACT

The lithium-sputtering yield from lithium and tin-lithium surfaces in the liquid state under low-energy, singly charged particles as a function of target temperature is measured by using the IAX (Ion-surface Interaction Experiment) facility. Total erosion exceeds that expected from conventional physical sputtering after accounting for lithium evaporation for temperatures between 200 and 400 °C. Lithium surfaces treated with high-fluence D atoms are bombarded by H<sup>+</sup>, D<sup>+</sup>, He<sup>+</sup>, and Li<sup>+</sup> at energies between 200 and 1000 eV and 45-degree incidence. Erosion measurements account for temperature-dependent evaporation. Results show the sputtering yield of lithium is anomalously enhanced to absolute values above unity as the temperature nears  $\sim 2.0 T_m$  (where  $T_m$  is the melting temperature of the sample). The enhancement of lithium sputtering is measured for all incident particle energies and exceeds sputtering levels predicted by linear cascade theory. Modeling with modified binary collision approximation codes suggests that two mechanisms are responsible for the enhancement: near-surface energy deposition and the nature of the binding between target atoms and the sputtered atom. Comparison to a low-vapor-pressure lithium alloy (0.8 Sn-Li) also results in nonlinear rise of lithium erosion as a function of temperature. Secondary ion-induced sputtered fraction measurements indicate a weak dependence with surface temperature.

**PACS codes:** 34.50.Dy, 52.40.Hf, 61.25.Mv, 69.49.Sf

**Keywords:** liquid lithium, sputtering, sputtered ions, thermal sputtering, fusion materials

**Corresponding authors:** J.P. Allain, [allain@anl.gov](mailto:allain@anl.gov) and D.N. Ruzic, [druzic@uiuc.edu](mailto:druzic@uiuc.edu)

## I. INTRODUCTION

The temperature dependence of lithium sputtering is important in many applications. These include: ion thruster physics, fusion plasma-facing components, extreme ultraviolet lithography, and lithium battery production. Engineering design criteria heavily depend on surface properties such as ion-induced sputtering and the effects of light impurities on the response of the surface to its environment.

From a fundamental point of view, investigating how a surface erodes as its temperature is increased can aid in our understanding of how atoms in a low-dimensional state (at the surface) evolve under both kinetic and thermodynamic changes. This information is particularly important for understanding interfacial phenomena such as a liquid-metal with its vapor.

By convention, physical sputtering (defined as the number of sputtered atoms per incident bombarding ion) does not have a strong dependence with temperature. In contrast, evaporation does have strong temperature dependence and is characterized by the heat of vaporization of a given material. Therefore a material in the liquid state irradiated by energetic charged particles well below its boiling point is not expected to erode any differently from its solid state.

The interaction between low-mass energetic charged particles and liquid lithium, from the standpoint of erosion, has received recent attention because of its application as a plasma-facing component (PFC) in fusion devices [1-6]. In addition, the possible use of lithium as an alternative EUV radiator in extreme ultraviolet lithography has also attracted interest. Recent experimental results of liquid lithium erosion in the linear plasma device PISCES-B showed enhanced erosion behavior with an increase in target temperature for low-energy, deuterium and helium bombardment [7-9]. The enhancement is measured to be substantially greater than

erosion by the expected lithium evaporative flux. This phenomenon was studied in IIAX (Ion-surface Interaction Experiment); a particle-beam facility that studies and simulates conditions found in plasma/wall environments of tokamak fusion devices. The enhancement of lithium sputtering with temperature was discovered even with an ion particle flux of about 3-4 orders of magnitude *lower* than that of linear plasma device experiments, for a variety of liquid-metals including Li, Sn, and Sn-Li.

The measurements in IIAX included variation of the incident particle energy at oblique incidence under various surface conditions (e.g., deuterium-treated and non-deuterium-treated surfaces). Oblique ion incidence at 45 degrees with respect to the surface normal simulates conditions at the edge of a tokamak fusion device. In addition, treatment with energetic D particles achieves simulated surfaces saturated with hydrogen isotopes. This is particularly important for lithium because of its high entrapment of hydrogen and, in fact, is one motivator for its application because it would, in principle, lead to low hydrogen isotope recycling and high edge temperature regimes in a tokamak fusion device [1,5]. The energy range of bombarding particles between 200 and 1000 eV in IIAX experiments is carefully selected to simulate expected energies for high edge temperatures characteristic of low-recycle regimes.

At room temperature and just above the Li melting point, sputtering results in IIAX resulted in little difference in lithium erosion [10]. In the measurements presented in this paper, however, as the surface temperature is increased beyond the lithium melting point, nonlinear erosion ensues, even when accounting for evaporation. This paper includes measurements from various light particles:  $H^+$ ,  $D^+$ ,  $He^+$ , and  $Li^+$  exposing Li and Sn-Li samples at 45-degree incidence with respect to the axis normal to the target. The singly charged ions are accelerated to energies near 200 eV and up to 1000 eV.

Investigation of lithium erosion also included sputtering measurements from a lithium-tin alloy (0.8 Sn-Li) whose vapor pressure is about three orders in magnitude *lower* than for pure lithium for temperatures investigated. This bimetallic system is useful in these nonlinear erosion studies for two primary reasons. First, the system has a very low vapor pressure; thus the evaporation flux is several orders of magnitude lower than sputtering near and above the melting point. Therefore, nonlinear erosion processes induced by ion bombardment are more clearly distinguished. Second, the eutectic alloy of Sn-Li has been found to have a Gibbsian-segregated Li surface layer at the temperatures studied here [11]. Since the depth of origin of sputtered particles originates in the top few monolayers, a comparison between liquid 0.8 Sn-Li and liquid Li could provide insight into the underlying mechanisms leading to nonlinear sputtering.

In addition to temperature-dependent erosion measurements, the ion-induced secondary sputtered fraction of lithium and tin-lithium was measured as a function of temperature. All surfaces were treated with a high fluence of D particles to simulate conditions in a fusion tokamak environment, although comparison is made to a pure lithium surface.

The paper begins with a section on linear and nonlinear sputtering and liquid-metal sputtering dependence on system temperature. The following section describes the experimental setup and modeling of liquid-metal sputtering. The paper continues with results and discussion and concludes with a summary and suggestions for future research.

### A. Linear and nonlinear sputtering

The linear dependence of the sputtering yield was developed by the work of Sigmund and Thompson [12-14]. The sputtering yield is defined as

$$Y \propto \frac{F_D(x=0)}{NU}, \quad (1)$$

where  $F_D$  is the deposited energy distribution at the surface ( $x = 0$ ) from charged-particle bombardment in the limit of high-energy (typically energies  $> 100$  eV),  $N$  is the number density of the target, and  $U$  is the surface barrier potential conventionally defined as the material's heat of sublimation. The energy deposited into atomic motion leads to the term collision cascade. If the collision density or the number of collisions per unit volume is small enough, then the damage process can be described by a simple binary event in which the struck atom is stationary during the collision and the energy deposition, on the average, can be modeled by a linear Boltzmann transport equation by Sigmund [12]. This type of linear cascade is characterized by the number of defects varying linearly with the total elastic energy deposited and the sputtering yield varying linearly with that part of the deposited energy at the surface.

As the elastic collision cross-section increases with incident ion mass and target mass, a higher recoil density of atoms will result in a higher rate of energy deposition. Eventually, linear cascade assumptions will fail, and a heavily disturbed region or high-density cascade will develop, leading to nonlinear sputtering. High-density cascades or energy spikes are characterized by deposited energy densities much larger than the normal thermal energy density. These energy spikes are deposited within  $10^{-13}$  to  $10^{-12}$  seconds, and collective effects associated with local damage will lead to nonlinear sputtering increases of the material.

Any nonlinear increase in the yield is therefore attributed to either an increase in  $F_D$  or an effective decrease in  $U$ . Attempts have been made to explain nonlinear increases in the sputtering

of certain high- $Z$  materials by surface degradation, leading to a decrease in  $U$  [15-17]. Therefore, with such sensitivity to the magnitude of  $U$ , care is needed to define the role of the surface barrier and the surface-binding model used to describe the sputtering process. Nonlinearity in the sputtering yield is also attributed to elastic-collision spikes (displacement spikes) or volumes of high density of deposited energy (high  $F_D$ ) where most of the target atoms are temporarily in motion [13,18-20]. In such cases the underlying assumptions that exist in linear cascade theory and Monte Carlo simulation codes based on the binary collision approximation fail to predict the underlying physics due to the low density of moving atoms in the cascade assumed in these models. One example is liquid-Li sputtering data of 700 eV  $\text{He}^+$  bombardment at 45-degree incidence [21].

Although elastic-collision spikes or energy spikes make a plausible argument for measured enhanced sputtering rates, their existence has very strict conditions with respect to the near-surface energy deposition:

$$\frac{\nu(E)}{N\Omega} > U, \quad (2)$$

where  $\nu(E)$  is the volume-integrated energy deposition near the surface,  $\nu(E) = \int F_D(\vec{r}, E) dV$  and  $\Omega$  is the slowing-down volume. Therefore, if a larger fraction of the energy is deposited in a smaller volume near the surface surpassing the cohesive energy or surface binding energy of the system,  $U$ , then conditions for energy spikes at the surface and consequently enhanced erosion can exist. These conditions can be met experimentally by heavy-ion bombardment at high energies, and in some cases, light-ion bombardment at low energies for oblique incidence on low heat of sublimation materials (e.g., Li, Mg, Ca, Na, K).

In addition to energy spikes, thermal spikes also have been known to lead to nonlinear sputtering. In terms of time scales, thermal spike phenomena will follow propagation of displacement (elastic-collision) spike phenomena [22,23]. In practice it is often difficult to discern between the two phenomena because they are closely connected through the dependence of damage on the deposited energy at the surface [16,20]. However, studies of sputtered energy spectra have identified several time-dependent regimes distinguishing ballistic mechanisms from thermal mechanisms during particle-induced sputtering [13,14]. For example, prompt collisional processes ( $10^{-15}$  to  $10^{-14}$  sec) and slow collisional processes ( $10^{-13}$  to  $10^{-12}$  sec) often are associated with elastic-collision phenomena. On the other hand, prompt thermal processes ( $10^{-12}$  to  $10^{-10}$  sec) and slow thermal processes ( $10^{-10}$  to  $10^{-9}$  sec) are known to be correlated with thermal spike and thermally associated phenomena [24-27].

Thermal spike models have been used to explain nonlinear sputtering of metals and insulators from a variety of bombardment situations [28-32]. Since the energy that appears in the prominent thermal pulse is localized initially to a single atom during initial bombardment in the model, the atom is set into vibration in a thermal spike, whereas it is displaced from its normal position and wanders for a distance in the displacement spike. Both thermal and energy spike phenomena are believed a few of the primary mechanisms dictating nonlinear erosion processes. Another mechanism, which enhances the energy density at the surface, is cluster-ion bombardment [33]. This mechanism cannot apply to experiments presented in this paper, however, because erosion induced by monomer bombardment is measured. A phenomenological model for thermal spike evolution is discussed and applied to the sputtering of liquid lithium in a later section.

## **B. Temperature dependence of physical sputtering for liquid metals**

The physical sputtering yield of a metal is weakly dependent on surface temperature because the surface cohesion energy of a metal has a very weak temperature dependence. Therefore, for a metal beyond its melting point, the physical sputtering yield is expected to depend little on temperature. Numerous examples of physical sputtering work and its dependence on temperature are given in the literature [14-18,26,28,30-32,34-44]. These differ mainly in the way energy is deposited during bombardment, with strong dependence on the thermodynamic and kinetic state of the condensed matter system.

A portion of this work attempts to provide a temperature-dependent sputtering model via the thermal spike model as discussed earlier. In addition, the thermal spike model has been successful in explaining sputtering of weakly bound condensed gas solids, a topic relevant in astrophysics [29,45]. Other results of temperature-dependent sputtering include the work of R.S. Nelson in the 1960s, who studied high energy sputtering of metals at elevated temperatures [46,47]. The sputtering yield was found to increase nonlinearly with temperatures  $T/T_m > 1.0$ .

Additional results showed weak temperature dependence for the physical sputtering yield. Besocke et al. conducted a series of experiments to determine the validity of a thermal spike model on temperature-dependent sputtering experimental results [48]. The experiments measured the differential sputter yield for 8 keV  $\text{Xe}^+$  ions on polycrystalline silver at normal and oblique incidence. The authors concluded that there was no significant thermal spike component in heavy-ion, low-energy sputtering and thus weak temperature dependence for sputtering. Behrisch and Eckstein simulated the temperature dependence of sputtering for silver at very low energies and found a weak sputtering yield increase with temperature [49]. The simulations were

carried out with the Monte Carlo code TRIM-SP, and the parameter varied as a function of temperature was the surface binding energy.

Other studies have carried out sputtering measurements from liquid metals, one in particular on liquid Ga-In [50-53]. However, the results did not show strong temperature dependence of the sputtering yield.

Although most work of both modeling and experiments shows a weak temperature for physical sputtering, some results suggest nonlinear enhanced sputtering correlated with an increase in target temperature or incident particle energy. Such enhanced sputtering effects have been measured only for heavy-ion, high-energy density cases [41,48,54-56] or for cluster-ion impact [33,57-59]. Other results have shown enhancements for heavy-ion, low-energy (<1 keV) bombardment [60,61]. Therefore, at low energies and bombardment with light particles (e.g., He or D in this paper), such enhanced erosion mechanisms are not expected and thus motivates the study established in this paper.

The fact that little evidence exists for strong temperature dependence of physical sputtering raises the following question: Under what circumstances, if any, does one expect the physical sputtering yield to strongly depend on temperature? Therefore, a system that has low heat of melting and low sublimation heat would be ideal to examine any temperature-dependent features. One system of interest is lithium and its alloys.

Lithium has a low melting point (180 °C), low heat of sublimation (1.7 eV), low heat of melting (0.03 eV), high vapor pressure, and low density, providing for an ideal system to study possible nonlinear sputtering phenomena. This approach is similar to studies conducted by deVries et al. [62], who worked with alkali-halide targets whose sputtered energy spectra more readily showed evidence of evaporative behavior at much lower incident particle energies than

did studies with gold, indicating that nonlinear behavior could exist for less-dense cascades with relatively low deposited energy distributions compared to more-dense cascades.

In turn, an alloy of lithium with another low melting point material, such as Sn, could also be a good candidate for nonlinear erosion studies. More important in the temperature range studied in this paper (200–400 °C) the vapor pressure of SnLi is about 4–5 orders of magnitude lower than that of lithium. Thus, the lithium alloy is an ideal system to compare nonlinear sputtering due to temperature, since evaporative fluxes will likely be undetectable. Lithium and tin-lithium systems are studied in this paper to determine whether any nonlinear erosion mechanisms exist when sputtering at various temperatures and incident particle energies above their melting point.

Experimental results presented here demonstrate the nonlinear erosion of lithium-based liquid surfaces when bombarded by energetic light particles. The temperature-dependent sputtering behavior shows signs of Arrhenius nature with an effective surface potential energy as the “activation barrier.” Both kinematic and thermodynamic dependences are carefully studied and experimental results discussed along with data on the temperature dependence of ion-induced sputtered ion fraction (IISIF) and hydrogen isotope retention. In addition, a comparison between hydrogen and deuterium bombardment is made to investigate isotopic dependencies.

## II. EXPERIMENTAL MEASUREMENTS OF LIQUID-METAL EROSION

### A. Experimental setup

IIAX has been designed to perform energetic particle-surface interaction studies on liquid metals, such as liquid lithium, liquid tin, and liquid tin-lithium [10,63-65] as shown in Figure 1. A Colutron ion source is used to create and accelerate gaseous or metal ions onto a  $0.066 \text{ cm}^2$  liquid metal target. The bombarding ions are mass-selected through an  $E \times B$  filter and decelerated near the target by a five-element cylindrical electrostatic lens system. Complete details of the system can be found in earlier papers [10,66]. A  $0.75 \text{ mm}$  thick and  $100 \text{ mm}^2$  lithium target is inserted in the main chamber containing argon gas at just above an atmosphere. The target can be rotated in order to provide variation in the angle of incidence; for these studies a 45-degree incidence was applied. A plasma cup is used to provide deuterium plasma cleaning of the target leading to the removal of any oxides or other impurities from the surface. This method also allows for deuterium implantation in liquid lithium, simulating plasma-facing wall conditions within a fusion reactor [10,67]. The irradiated fluence of D atoms in liquid lithium is of the order of  $10^{17}$ - $10^{18} \text{ D/cm}^2$ , comparable to doses in a tokamak environment.

A dual quartz crystal microbalance dual-crystal unit (QCM-DCU) is rotated in front of the target to collect the sputtered flux, measuring the absolute sputtering yield. This dual QCM technique is described in earlier papers [64,66]. The QCM unit is mounted on a manipulator, and thus its spatial and angular position with respect to the target is known. Figure 2 shows a sample trace of the frequency difference,  $\Delta f$ , of the dual QCM unit against time plotted with ion current on the sample for  $700 \text{ eV He}^+$  45-degree incidence. The figure plots the QCM frequency difference in hertz on the left ordinate and the beam current measured on the liquid lithium sample during sputtering on the right ordinate. The curve with the slope-fitting lines is the QCM

crystal difference data. The QCM crystal frequency difference in hertz and the beam current on the liquid metal sample in amps are plotted over time. The frequency difference has four parts: when the initial signal measuring evaporation (labeled 1); when the beam is turned on, the signal measures sputtering and evaporation (labeled 2); when the beam is turned off, some oxidation on the QCM crystal as it evaporates (labeled 3); and when steady-state evaporation signal is reached before sputtering (labeled 4).

A small high-temperature, high-vacuum substrate heater is used to heat the target past its melting point to temperatures ranging from 200 °C to about 400 °C. Measurements of liquid-Li and liquid-Sn-Li sputtering are taken under equilibrium conditions at each target temperature of interest. Therefore, background evaporation is measured before and after ion bombardment at each particular incident energy and surface temperature. A tantalum evaporative shield is floated on top of the liquid metal target. As the sample is heated, a thin oxidized “slag” layer is formed and is removed with an in situ mechanical arm. The arm includes a thermocouple, which also measures the temperature of the liquid metal as the arm is partially immersed in the liquid metal during slag removal. Although two thermocouples are utilized to measure the liquid metal temperature, error still exists from the uncertainty of the temperature measurement because heat transfer will occur from the surface of the liquid metal to the stainless steel arm or tantalum shield. Therefore, error bars of the order of 20–30% are included in the temperature values.

The incident ion flux to the target averages values in the order of  $10^{13}$  -  $10^{14}$  ions/cm<sup>2</sup>/sec. The evaporative flux from liquid lithium is  $5.1 \times 10^{11}$  atoms/cm<sup>2</sup>/sec (at 200 °C) and can reach levels of  $10^{13}$  atoms/cm<sup>2</sup>/sec or higher at temperatures near 400 °C. The sputtered flux levels vary from  $10^{12}$  and up to  $10^{14}$  Li atoms/cm<sup>2</sup>/sec. Molecular dynamics calculations have found that the sticking coefficient of thermalized atoms is lower than for sputtered particles with peak

energies between 5 and 10 eV [68] at temperatures greater than the melting point of lithium. Therefore, the frequency difference temporal slope ( $\Delta f/\Delta t$ ) between evaporated and sputtered fluxes during ion bombardment is measurable.

At temperatures near and above 450 °C, the physical sputtering and evaporative fluxes are difficult to discern since the evaporative flux is equal to or greater than the sputtered flux. The partial pressure of impurities in the system is monitored with a quadrupole gas analyzer, and partial pressures of oxygen and hydrocarbons are kept below  $10^{-8}$  Pa. Typical total base pressures before the sample is exposed to the beam are  $10^{-6}$  to  $10^{-5}$  Pa. During each lithium-sputtering yield measurement from liquid Li or liquid Sn-Li samples, the ion-induced secondary ion sputtered fraction (IISIF) is measured. This procedure is done by biasing the sample negatively over a range of voltages and measuring the total ion current. Details of this measurement are included in earlier work [66]. The IISIF is measured to be about 66% for solid and liquid Li and liquid Sn-Li surfaces. For solid Sn-Li surface the IISIF is about 10%. These results are discussed later in the paper.

## **B. Data analysis**

Analysis of the absolute lithium-sputtering yield from both liquid lithium and liquid tin-lithium samples correlates the time-dependent frequency variation in the crystal signal with the time period of ion beam dose. The calculation of the absolute sputtering yield is then possible after accounting for sputtering of QCM deposited material by incident, highly energetic reflected particles, sticking coefficient of sputtered atoms onto the QCM crystal, and the secondary ion fraction of sputtered atoms. Details of data analysis and calculations are discussed in earlier work using identical QCM-DCU system for both liquid Li and liquid Sn-Li sputtering at temperatures

near the melting point [10,63]. A mass balance between the mass loss from the lithium sample and the mass gained on the QCM deposition crystal results in the expression for the absolute sputtering yield in units of Li atoms/ion:

$$Y = \frac{2 \cdot N_A}{D f_i S^{QCM} \Omega m_{Li_2O}} \frac{\Delta f}{f} M_{crystal} + R_j^{QCM} Y_j^{QCM} \Omega_j . \quad (3)$$

$D$  is the total ion dose;  $S^{QCM}$  is the sticking coefficient defined as  $1 - R_j^{QCM}$ , where  $R_j^{QCM}$  corresponds to the reflection coefficient for sputtered species  $j$  off the QCM crystal surface and is calculated by VFTRIM-3D[69];  $Y$  is the absolute sputtering yield in sputtered atoms or particles per ion;  $\Omega$  is the fraction of the normalized distribution of sputtered particles subtended by the QCM crystal;  $f_i$  is a factor accounting for the ion fraction of sputtered species (sputtered secondary ions) ranging from 1.5 to 1.8; and  $m_{Li_2O}$ , the mass of lithium oxide deposited on the QCM deposition crystal in grams/mol with  $N_A$ , is Avogadro's number ( $6.02 \times 10^{23}$  atom/mol). A factor of 2 is included because two moles of  $Li_2O$  are produced for every four moles of Li consumed. The frequency change,  $\Delta f$ , is measured from the raw frequency difference between the deposition and reference crystal data.  $M_{crystal}$  is the mass of the crystal given by the manufacturer, and  $f$  is the initial frequency of the QCM crystal.

Expression (3) does not include the partial sputtering yield of Sn, for the case of Sn-Li sputtering, for two reasons. The sputtering threshold for pure Sn is high near 200–300 eV because of its high elemental surface binding energy. At a 45-degree incidence the sputtering yield of Sn tops 10–20% at energies of 500–1000 eV, according to simulations with VFTRIM-3D. In addition, XPS measurements show that 99.6% of the mass deposited on the QCM crystal is oxidized lithium. These measurements confirm measurements by R. Bastasz of tin-lithium in liquid phase, where lithium atoms segregate to the surface [11,70], and thus lithium and *not* tin is

the ion beam-facing surface. In addition, beyond the melting point of Sn-Li, the sputtered secondary ion fraction is about 66% (equivalent to pure Li), thus implying that the first few monolayers are made up of pure Li in the liquid Sn-Li alloy eutectic. This result is consistent with measurements of lithium surface segregation made for Li-Al and Li-Cu systems by Krauss and Gruen [71].

### III. MODELING OF LIQUID-METAL SPUTTERING

Currently no self-consistent model exists that predicts lithium nonlinear sputtering with temperature. Several models have been developed, including a modified BCA (binary collision approximation)-based surface model, a hybrid BCA and molecular dynamics model, and a model that accounts for the generation and erosion of adatoms formed on liquid surfaces [9,21,68,72].

None of these models have a complete self-consistent picture that explains the mechanism responsible for nonlinear erosion from liquid Li surfaces induced by low-energy, light-particle bombardment as a function of system ambient temperature. In fact, these models fail to provide *a priori* the description of liquid-metal sputtering without use of approximations or fitting to the experimental data they are attempting to predict. This difficulty is primarily due to the seemingly multibody behavior inherent in the erosion of liquid Li induced by low-energy, light-particle bombardment at grazing incidence. In addition, this difficulty is exacerbated by the surface structure developed on liquid-metal surfaces at spatial scales near the sputter depth. Although models designed to simulate temperature-dependent physical sputtering from liquid-metal surfaces remain arguably at their infancy, their use helps elucidate surface mechanisms that could help explain experimental evidence for nonlinear erosion of liquid Li and Sn-Li with temperature. This section presents a semi-empirical theoretical model that combines a collisional

(kinematic) and thermodynamic form of liquid lithium sputtering. The model is based on a localized thermal-spike mechanism described by a localized volume of mobile atoms characterized by low cohesive energy. The semi-empirical model is advantageous in that it provides a fast and efficient method to predict liquid-metal sputtering as a function of temperature without the need for computationally expensive molecular dynamics runs with approximate potentials or approximations of surface potentials used in Monte Carlo BCA-based simulation methods.

### A, Semi-empirical modeling of collisional sputtering

To incorporate the energy dependence of ion-induced sputtering, we use the BSY (Bohdnansky-Sigmund-Yamamura) model for expressing the *collisional* sputtering yield term:

$$Y(E, \theta) = \Lambda F_D(E, \theta, x = 0). \quad (4)$$

With the material factor,  $\Lambda$ , and  $F_D(E, \theta, x = 0)$  the *surface-deposited* energy as defined by Jakas [73].

This expression by Sigmund et al. [74] is calibrated to experimental data, and appropriate scaling factors are applied, resulting in an empirical relation known as the Bohdansky formula [12,75], for normal incidence:

$$Y(E_o, \theta = 0^\circ) = Q S_n^{KrC}(\varepsilon) \left[ 1 - \left( \frac{E_{th}}{E_o} \right)^{2/3} \right] \left( 1 - \frac{E_{th}}{E_o} \right)^2. \quad (5)$$

In this case  $Q$  is known as the yield factor and is expressed as

$$Q = \frac{0.042}{U} \alpha(M2/M1). \quad (6)$$

Here  $s_n^{KrC}(\varepsilon)$  is the nuclear stopping cross-section normalized to the reduced energy,  $\varepsilon$ . The reduced energy is the ratio of  $E_o$  and  $E_{TF}$ , where  $E_{TF}$  is the energy in the center-of-mass system for a head-on collision with the screening radius as the nearest approach. The factor  $\alpha$  is a dimensionless number dependent on the mass ratio  $M_2/M_1$ , incident energy, and angle of incidence [12]. Lastly,  $E_o$  is the incident particle energy,  $U$  is the surface binding energy, and  $E_{th}$  is the threshold energy where the sputtering yield becomes zero.

This empirical relation can be expressed as a function of the angle of incidence. A revised formula, which uses the treatment by Yamamura et al. [76], results in the relation

$$Y_{coll}(E_o, \theta) = Qs_n^{KrC}(\varepsilon) \left[ 1 - \left( \frac{E_{th}}{E_o} \right)^{2/3} \right] \left[ \left( 1 - \frac{E_{th}}{E_o} \right)^2 \frac{1}{(\cos \theta)^f} \exp \left[ f \left( 1 - \frac{1}{\cos \theta} \right) \cos \alpha_{opt} \right] \right]. \quad (7)$$

Values for  $f$  and  $\alpha_{opt}$  are used as fitting parameters. A revised approach adapted by Garcia-Rosales et al. [75] uses an analytical fit proposed by Yamamura [76] for the value of  $f$ . The empirical expression results in a weak function of  $f$  with the incident particle energy,  $E_o$ , for all  $M_2/M_1$  ratios. However, experiments [75] show that  $f$  is a strong function of the incident particle energy,  $E_o$  for ratios less than  $M_2/M_1 = 6$  down to self-sputtering values. Therefore, empirical fits to these experimental data in the range of  $E_o = 100 - 1000$  eV are used for values of  $f$  for the combinations of D, He, and Li bombardment of solid lithium [66]. These fits make up the semi-empirical model of the collisional erosion term in this paper.

## B. Semi-empirical modeling of thermal sputtering

Nonlinear sputtering phenomena can be attributed to thermal spike phenomena in the high-energy, heavy-ion bombardment limit. Similarly, one can utilize such models for the case of low sublimation energy materials (e.g., lithium or magnesium) at moderate particle energies and collisional sputtering components after the treatment by Thompson [13,77]. The thermal sputter yield is defined as

$$Y_{th}(E, \theta, T^*) = \Lambda_{th}(T^*) F_D(E, \theta, x = 0), \quad (8)$$

where  $\Lambda_{th}(T^*)$  is the thermal material factor, and  $F_D(E, \theta, x = 0)$  the *surface-deposited* energy as defined earlier. The thermal material factor is related to the quasi-equilibrium energy distribution in the induced spike with average energy  $\Theta$  per atom,  $f(E_o, \Theta)$ , by the energy distribution of recoil atoms,  $f_r(E_o, \Theta)$  with initial energy,  $E_o$ , defined as

$$f_r(E_o, \Theta) = \psi \cdot \tau \cdot N\Omega \cdot f(E_o, \Theta) \cdot dE_o, \quad (9)$$

where  $\psi$  is the recoil particle current,  $\tau$  is the time constant for the induced spike temperature, and  $\Omega$  is the slowing-down volume. The average energy per atom also satisfies the condition that  $\Theta > U$ , where  $U$  is the cohesive energy of the system in the spike volume,  $N\Omega$ . The energy distribution is related to the thermal material factor by definition of the sputter yield and emission probability:

$$\Lambda_{th}(\Theta) = \frac{\tau}{4\pi\Theta} \int dE_o \nu_o f(E_o, \Theta) \int d\Omega_o |\cos \theta_o| P(E_o, \theta_o), \quad (10)$$

where  $P(E_o, \theta_o)$ , is the emission probability and is defined to be valid as

$P(E_o, \theta_o) = F \left( \frac{E_o - U^*}{\cos^2 \theta_o} \right)$ , where  $U^*$  is the thermodynamic sublimation energy at the melting

point. The quasi-equilibrium energy distribution in the spike is defined as

$$f(E_o, \Theta) = C \cdot E^{1/2} \exp\left(\frac{-3E_o}{2\Theta}\right). \quad (11)$$

The average energy per atom is defined as

$$\Theta \approx \frac{\nu(E)}{N\Omega} = \frac{3}{2} k_B T^* . \quad (12)$$

Combining these relations, one derives the thermal material factor as a function of  $T^*$ :

$$\Lambda_{th}(T^*) = \frac{\tau}{\sqrt{\frac{9\pi}{2} M k_B T^*}} \exp\left(\frac{-U^*}{k_B T^*}\right) \quad (13)$$

Therefore an expression for the thermal sputter yield as a function of the deposition energy distribution at the surface,  $F_D(x=0)$ , and  $T^*$ , is obtained:

$$\text{Given: } F_D(E, \theta, x=0) = \alpha(M2/M1) f(\theta) NS_n(E),$$

we get

$$Y_{th}(E, T^*, \theta) = \frac{\alpha(M2/M1) f(\theta) \tau \cdot NS_n(E)}{\sqrt{\frac{9\pi}{2} M2 k_B T^*}} \exp\left(\frac{-U^*}{k_B T^*}\right). \quad (14)$$

$T^* = T + T_s$ , with  $T_s$  defined as the spike temperature due to nonlinear deposition of energy at the surface at ambient system temperature,  $T$ . This temperature profile can be derived from the one-dimensional heat equation in cylindrical coordinates and its result is

$$T_s(r, t) = \frac{Q'}{\rho C_p} \frac{1}{8(\pi K t)^{3/2}} \exp\left(\frac{-r^2}{4Kt}\right). \quad (15)$$

### **C. Combination of thermal and collision sputtering semi-empirical models**

Semi-empirical modeling of sputtering as a function of temperature consists of summing a thermal sputtering term and a collisional sputtering term. This approach was adopted by Thompson et al. [13] in describing thermal sputtering mechanisms. Adding both the collisional and thermal sputtering terms according to the Sigmund and Thompson models, we obtain what is defined in this paper as the BSY-thermal model:

$$Y = Y_{coll} + Y_{th} . \quad (16)$$

## **IV. RESULTS AND DISCUSSION**

Presented in this section is the lithium-sputtering yield measured in IIAX from bombardment of various singly-charged monoenergetic incident particles on liquid lithium and liquid tin-lithium at oblique incidence. Also presented is data on the ion-induced secondary ion sputtered fraction measured for both liquid lithium and liquid tin-lithium. In addition, we discuss the determination of how the effect of deuterium treatment of liquid lithium samples on the lithium-sputtering yield varies with temperature.

### **A. Bombardment by helium**

Figure 3 shows the  $\text{He}^+$  bombardment of liquid lithium measured as a function of incident particle energy for various temperatures at oblique incidence. Helium is used as a control experiment because chemical effects with the lithium surface are absent and analysis of any measured nonlinear erosion is facilitated. Experiments in IIAX use relatively low ion fluxes and fluences believed to be below the threshold for bubble formation stability in liquid lithium.

The linear sputtering yield from the BSY model (without temperature effects) is shown in [Fig. 3](#) for comparison. As the temperature is increased beyond the lithium melting point, the lithium-sputtering yield is enhanced beyond the level predicted by linear sputtering theory. The functional dependence of the lithium-sputtering yield on incident particle energy is not as strong as its dependence on temperature. Vaulin measured a similar functional dependence of the sputtering yield with temperature [60]. In addition, similar liquid Li weak energy dependence response was found for lithium interaction with T-11M tokamak [78] and, more important, stronger temperature dependence. The result, shown in [Fig. 3](#) from our 2001 experiments, measured and predicted this behavior and is only one of several experimental verifications of lithium's propensity to sputter anomalously with temperature.

At temperatures near the melting point of lithium ( $\sim 200\text{ }^\circ\text{C}$ ), the maximum lithium-sputtering yield is reached for incident particle energies near 500 eV. As the temperature is increased, the maximum shifts to lower energies, although this trend is difficult to confirm because of the lack of ion-beam data at energies below 200–300 eV. However, liquid-lithium sputtering data at 75 and 150 eV in PISCES-B shows magnitudes larger than at the 200–300 eV energies in this work, indicating that perhaps a shift does exist.

Earlier data of sputtered energy distributions by Thompson showed similar behavior for conditions where the near-surface cascade was large. The spectrum of energy ejecta typically

showed shifts to lower energies and a corresponding increase in magnitude. Recent sputtered energy distribution experimental data from liquid Li surfaces under ion irradiation showed similar shifts of the peak energy [7]. The data in Fig. 3 does not show a strong energy dependence, and this situation may imply a thermodynamic component of the lithium non-linear erosion in addition to a collisional mechanism. However, measured sputtered energy spectra under lithium enhanced erosion conditions show peak energies between 0.1 and 1.0 eV in the range of 200–400 °C, distinctly large compared to typical thermal emission energies (i.e., 0.025 to 0.1 eV) [7]. Therefore, it is unlikely that the emission of atoms in the non-linear regime is thermal; on the contrary, the measured emission spectra imply a combined model of mobile atoms due to an excited thermodynamic state and collisional sputtering.

### **B. Bombardment by hydrogen (H, D)**

Bombardment of liquid lithium by hydrogen and deuterium singly charged particles is shown in Figs. 4 and 5. Nonlinear erosion of lithium is again detected. Bombardment with hydrogen is complicated by possible chemical effects between hydrogen and lithium. In addition, since the lithium surface is treated with D-plasma *prior* to ion bombardment, interaction of energetic hydrogen with implanted H particles could lead to complications in data interpretation. Nevertheless, similar results to those with He<sup>+</sup> bombardment have been obtained. A nonlinear erosion rise is obtained at temperatures higher than the melting point of lithium. The energy dependence of lithium sputtering is noticeably weaker than the yield's temperature dependence. This result indicates that the nonlinear erosion mechanism is not inherently chemical. In addition, although at these fluences no bubble formation of inert implanters is expected (e.g., He), the hydrogen data clearly shows that the nonlinear erosion is *not* due to bubble formation

since hydrogen is highly soluble in liquid lithium. Cases for surface blistering due to hydrogen bombardment have been observed, but these have thresholds of very high ion fluxes, orders of magnitude higher than the  $10^{13}$ – $10^{14}$  ion/cm<sup>2</sup>/sec fluxes in these experiments.

Moreover, the measured nonlinear erosion has no isotopic dependence when comparing lithium sputtering results between H and D. Thus, lithium erosion must be due to a combination of the local temperature state of the system and the energy imparted by the incident bombarding particle near the surface. Irradiation by H, D, or He is considered light-particle bombardment. In order to compare to a case where the bombarding particle mass is equal or greater than the lithium target, measurements with lithium ions were completed under similar conditions.

### **C. Liquid lithium self-sputtering**

Bombardment by lithium ions is a good case to study and compare with D and He irradiations. In this case we do not expect any stability for bubble formation and in addition any strong chemical effects, detectable by IAX diagnostics. Lithium sputtering from self-bombardment is shown as a function of temperature for various incident Li ion energies in Fig. 6 and as a function of impact energy in Fig. 7 for various temperatures. The enhancement is also found for self-bombardment as in the case of helium or hydrogen bombardment. This indicates that the underlying mechanism for erosion enhancement with temperature may not necessarily be due to inert gas bubble formation in the near-surface region followed by microexplosions, since that cavity formation and stability would be absent when liquid lithium is bombarded by lithium particles. In addition, the enhancement increases at a larger rate compared to D or He bombardment. This increase indicates that the enhancement mechanism is also connected to

collision dynamics and the way energy is deposited near the surface (a non-equilibrium process) as opposed to simply a thermodynamic process.

Lithium self-bombardment atomistic simulations with molecular dynamics were conducted and demonstrated that the recoil angular and energy distributions played a key role in how energy near the surface is deposited and how this changes with temperature [68]. In addition, the simulations also showed that the nature of the binding of sputtered lithium atoms to target atoms just before being emitted has a temperature dependence. The enhancement of lithium sputtering is also evident when plotting the lithium-sputtering yield against the incident particle energy for various temperatures. As in the case for D and He bombardment as the temperature of the surface is increased the maximum of the  $Y(E)$  curve is shifted to lower energies. This shift again confirms that the underlying mechanisms are collisional and corroborates low-energy measurements in PISCES-B discussed earlier. In order to further elucidate on whether the underlying mechanism is purely collisional or thermodynamic, a material with low vapor pressure is chosen for study.

#### **D. Temperature dependence comparison to liquid SnLi sputtering**

The results of lithium-sputtering from both lithium and tin-lithium targets are shown in Fig. 8 for 300–1000 eV  $\text{He}^+$  and 700 eV  $\text{D}^+$  ions at 45-degree incidence. The results show an enhancement in the lithium-sputtering yield as the target temperature is increased from the liquid-metal melting point up to temperatures near  $2T_m$ . The lithium-yield dependence on temperature is stronger than is the dependence on the incident particle energy for both surfaces. The lithium-sputtering yields from He and D bombardment of tin-lithium targets also show an

enhancement, although the threshold for nonlinear sputtering seems to be at a higher target temperature, near 375 °C. The striking results shown here indicated that for these temperatures, the vapor pressure of Sn-Li is undetectable by the QCM-DCU diagnostic. In addition, the nonlinear erosion yield shown is not due to any evaporation-related mechanism, thus indicating that nonlinear erosion is possible with light particle bombardment (e.g., He and D). Earlier results with D, He, and Li bombardment on Sn-Li just above its melting point showed yield enhancement due to strong backscattering of light-particle bombardment reaching levels beyond those of pure lithium sputtering.

The effect of D implantation on lithium sputtering from liquid Sn-Li surfaces also requires some discussion. From the temperature-dependent sputtering results and XPS data on the collector crystal, it is evident that lithium is the dominant species during sputtering and that the top few monolayers are made up mostly of lithium. This is indirect evidence that lithium, being the lower surface tension component at 390 mN/m (525 mN/m for Sn), segregates to the alloy surface in the liquid state viz Gibbsian segregation. This phenomenon was measured with low-energy ion scattering spectroscopy by Bastasz and Whaley for the same temperature range we investigated [11]. However, we find that for Sn-Li in the liquid state, the effect of D exposure does not seem to affect the measured sputter yield of lithium. This may be indirect evidence of low retention levels of hydrogen atoms in Sn-Li surfaces in the liquid state, even though the first few monolayers may resemble a pure liquid Li surface.

### **E. Inverse temperature behavior of liquid Li sputtering**

Both the thermodynamic behavior and kinematic behavior of lithium in the liquid state have been discussed in earlier sections. However, it is insightful to study the inverse-temperature behavior of lithium sputtering as it relates to incident energy, incident mass and incident flux. Figure 9 shows the inverse-temperature dependence of the lithium sputter yield parametrized with incident particle energy to weigh the kinematic vs thermodynamic nature of the enhanced erosion. Fig. 10 shows the inverse-temperature dependence of the lithium sputter yield parameterized with incident flux for several energies and incident mass, at 700 eV impact energy. The lithium sputter yield demonstrates an Arrhenius-like behavior at the onset of nonlinear erosion. This is particularly evident when varying the impact energy. Figure 9 also compares the case for a non D-sat lithium surface. The onset of nonlinear erosion with temperature is located at nearly the same temperatures, indicating a thermodynamic-dominated mechanism. In Fig. 10(a) the lithium sputter yield shows two distinct features. One is the onset of nonlinear erosion when comparing impact energies. In this case we compare PISCES-B experimental data of 175 eV He<sup>+</sup> bombardment of liquid Li with an ion flux ranging from 0.5-1.0 x 10<sup>18</sup> cm<sup>-2</sup>s<sup>-1</sup>. The onset for PISCES-B data is found near 0.00175 1/K and for IIAX data at 700 eV at about 0.00225 1/K. In addition, the IIAX experimental data incident He ion flux (<10<sup>14</sup> cm<sup>-2</sup>s<sup>-1</sup>) is more than four orders of magnitude lower than that used in PISCES-B, and, as shown, the rate of increase of the lithium sputter yield with temperature is slower by a factor of about 1.44. This enhancement with incident flux may be related to ion-induced near-surface shock waves leading to higher rate of increase of the lithium sputter yield with temperature. The comparison between IIAX and PISCES-B experimental data is valid even though the impact energies are different, as demonstrated by data from Fig. 9 of the invariance of the lithium temperature-dependent rate increase in yield with impact energy. Figure 10(b) shows that the dependence on

incident mass does not vary the onset of liquid Li non-linear erosion with temperature at constant impact energy of 700 eV. This comparison also demonstrates that thermodynamic-dominated near-surface mechanisms are responsible for the nonlinear erosion behavior of liquid Li sputtering. The kinematic dependence of liquid Li sputtering is manifested in the shift of absolute sputter yield level, as shown when varying the incident particle mass from 1 amu (H) to 6.9 amu (Li). Further work will study the enhancement of liquid Li sputtering as a function of heavy ions in the near future.

#### **F. IISIE vs T for $D^+$ , $He^+$ and $Li^+$ bombardment of liquid Li and SnLi**

The ion-induced secondary ion emission fraction of a metal is known to strongly depend on the chemical state of its surface [79,80]. Previous measurements of solid lithium sputtering by  $D^+$  and  $He^+$  bombardment showed that the IISIE for lithium was 0.66 Li ions/ atom [66]. Basic models exist for estimating the probability of secondary sputtered ions from particle bombardment. These models have been coupled recently with molecular dynamics simulations for the liquid Li system [72]. These show consistent results of large IISIE for liquid lithium. Figure 11 shows the result of IISIE experiments for D-treated liquid Li IISIE from 700 eV  $He^+$  bombardment as a function of surface temperature. The IISIE does not show a strong temperature dependence and does not depend on the bombarding species. The lack of variation between in IISIE from  $D^+$  bombardment compared to He or Li is probably due to the large amount of deuterium already present on the liquid Li surface prior to particle bombardment. This result is important when assessing the role of the IISIE in operation with a liquid Li surface in a fusion reactor. The IISIE will remain high during particle bombardment at an operating temperature range between 200 and 400 °C and apparently higher.

Figure 12 shows results for IISIE from 700 eV  $\text{He}^+$  bombardment of liquid Sn-Li as a function of temperature. This experiment clearly indicates, from the standpoint lithium sputtering, that the nature of the Sn-Li surface dramatically changes as the temperature is raised beyond the thermodynamic melting point of the metal alloy. This is yet additional evidence of Li segregating to the liquid alloy surface, as discussed previously. Moreover, the secondary ion fraction is a phenomenon whose spatial scale is a few monolayers from the surface, and thus the large secondary ion fractions found for temperatures beyond the melting point are not surprising in the context of our data from pure liquid-Li surfaces at similar temperatures. One interesting result from this figure is at the solid phase of Sn-Li. There is a measurable difference in secondary ion fraction when bombarding with  $\text{D}^+$  compared to  $\text{He}^+$ . Recall that both in [Figs. 11 and 12](#), the surface is treated with deuterium for fluences corresponding to 1:1 D to Li uptake. For solid phase Sn-Li, however, the secondary ion fractions are quite different from those of D-sat. liquid Li. The consequence of this is that during  $\text{D}^+$  bombardment of Sn-Li, the secondary ion fraction is larger than during bombardment with  $\text{He}^+$ . This is consistent with the strong dependence of the secondary ion fraction on the chemical state of an alkali surface.

### **G. Role of D saturation on liquid Li surfaces**

Figure 13 shows physical sputter yield results for  $\text{He}^+$  bombardment of liquid Li as a function of sample temperature and deuterium exposure fluence. These experiments were designed to understand the role D saturation had on the sputtering response of liquid Li under  $\text{He}^+$  bombardment. All of the temperature-dependent data were taken at 700 eV and 45-degree incidence. Several important aspects of these results are worth discussing. First, we find that as

the temperature rises beyond the melting point of liquid Li (1.5 times the melting temperature), the erosion resembles that of a surface not treated with D. This is likely due to D diffusing away from the surface of liquid Li. On an atomic scale, an atom in the liquid state is likely to migrate through fluctuations in density arising from the thermal motion of surrounding atoms. In addition, we found that the amount of deuterium atoms implanted at the liquid Li surface has a strong effect on the erosion behavior under particle bombardment. For example, we found that we needed D fluences above  $10^{17}$  D/cm<sup>2</sup> to reach saturated conditions at the liquid Li surface at temperatures above 200 °C. Therefore, we exposed two additional samples; one to  $3 \times 10^{17}$  D/cm<sup>2</sup> for several temperatures between 200 and 400 °C and  $5 \times 10^{16}$  D/cm<sup>2</sup> at 200 °C using a hollow cathode deuterium discharge with a bias of about 300 V. At 200 °C we find that the sample exposed to the least amount of deuterium, erodes higher, indicating the preferential sputtering effect we indicated earlier in this paper. As the deuterium content at the surface increases, we find that the total *lithium* sputtering decreases. The next case was to increase the temperature of the sample to a given level and then prepare with D exposure before irradiating with 700 eV He<sup>+</sup> and measuring sputtering. We find that at higher temperatures, D implanted has a net migration *away* from the liquid Li surface as its sputtering reaches similar levels to non-D-saturated liquid Li surfaces. This result, however, could also be interpreted by the fact that at temperatures near 400 °C, distinguishing between *evaporated* and *ion-induced sputtered* atoms becomes more difficult because of the comparable magnitudes of vapor and incident ion flux.

Another important result is that for a pure Li surface under the ion flux levels used ( $\sim 10^{13}$ - $10^{14}$  He<sup>+</sup>/cm<sup>2</sup>/sec) the enhancement of sputtering with temperature is not as pronounced. This result is particularly important in understanding the collection mechanisms involved in the measured enhancement of lithium sputtering from D-saturated liquid Li surfaces presented. The

large enhancements measured were mostly for D-saturated samples. [Figure 13](#) shows the only data as a function of temperature for a pure liquid-Li surface. The enhancement with temperature could be also indirect evidence that D atoms are readily diffusing away from the liquid Li surface were over 90% of the sputtered atoms emanate. Further studies must address the role of hydrogen isotopes in liquid Li surface erosion properties. Moreover, this high mobility of D atoms in liquid Li is indicative that D is not reacting with liquid Li as evidenced by thermodynamic equilibrium data showing that a maximum D saturation of 10% is reached at temperatures between: 200 and 400 °C [81]. Therefore, another explanation is that the implanted deuterium is in solution with Li and that LiD formation has been suppressed by another mechanism. Independent results support these findings; for example, deuterium retention studies in T-11M CPS found deuterium removal from liquid Li for temperatures above 320 °C—a temperature much lower than the expected LiD decomposition of 685 °C, thus suggesting that D atoms may be only dissolved in the liquid Li matrix. Similar results using thermal desorption mass spectrometry were found by deuterium retention studies by Baldwin et al. [82], except that LiD formation was found as the temperature was kept at 400 °C for at least two hours. Recent molecular dynamics results of hydrogen impact in liquid Li by Ruzic et al. have discovered an interesting behavior in which implanted H atoms segregate and coalesce into clusters without reacting with lithium atoms in the liquid matrix. This may be an initial indication of an explanation for the nature of hydrogen isotope bonding and mobility in liquid Li using atomistic simulations and perhaps an explanation of the discrepancy between earlier results of D retention in liquid Li. This intriguing phenomenon requires further computational study by atomistic simulations because, experimentally, this effect may be quite difficult to measure.

Figure 13 also presents thermal sputtering yield model fits to the experimental data for both cases of 700 eV He<sup>+</sup> on a non-D-saturated liquid Li surface and one where the D:Li concentration is equal at the surface. The semi-empirical model uses minimal use of fitting parameters and these are derived from detailed semi-analytical models including the BSY model presented earlier in the paper. The thermal sputter yield model does a good job of fitting the data, and we find that both curves approach each other as evaporative mechanisms dominate at temperatures beyond 723 K, as expected. The form of the thermal sputter yield model follows the qualitative form of Vaulin and Sigmund; the main difference is that the cohesive energy is defined to be disrupted by the surface deposited energy in the liquid, thus allowing for the thermodynamic approximation that:  $\Theta \approx \nu(E)/N\Omega = 3/2 k_B T$ .

## V. CONCLUSIONS

The temperature dependence of lithium sputtering in the liquid state has been investigated in experiments using low-mass charged particles and under self-sputtering. Both thermodynamic and kinematic effects are found to be responsible for the enhancement, although thermodynamic mechanisms are dominant. Lithium enhancement was studied by variation of several incident parameters including impact energy, incident mass, and comparisons with incident ion flux. The onset of lithium sputtering enhancement is found to occur at temperatures near 300 C, and the rate of increase of the yield with temperature is dependent only on incident ion flux and moderately with incident ion mass. A semi-empirical model developed to predict the temperature-dependent behavior couples both kinematic and thermodynamic effects. The thermodynamic behavior resembles that of Arrhenius behavior, although this behavior needs to be assessed further. The model assumes a localized damaged region characterized by highly

mobile atoms with reduced coordination number at the liquid/vapor interface. The incident ion flux dependence shows that even for about a four-order-of-magnitude difference in ion flux, the rate of increase of the lithium sputter yield with temperature changes at most by 44%. The difference could be due to near-surface localized shock-wave expansion effects. All experimental data of temperature-dependent lithium sputtering were taken with mass-loss diagnostic systems. Therefore, the enhanced population of sputtered particles could be due to the generation of small clusters during bombardment and shock wave generation, and more prevalent at higher incident ion fluxes. The study of cluster emission from liquid Li surfaces is a topic of future work.

In addition to the study of the temperature dependence of the lithium sputter yield, the secondary ion fraction induced by incident ions was also studied and compared for two material surfaces. A monotonic increase in the secondary ion yield was found with temperature. A more pronounced dependence was found when comparing a lithium alloy, 0.8 Sn-Li with a liquid Li surface. In this case once the alloy reached its melting point, a segregated Li layer was formed and the surface behaved similarly to liquid Li.

The effect of deuterium saturation of various liquid Li and alloyed surfaces was also studied. Results show that deuterium effectively decreases the absolute sputter yield of Li. Deuterium coverage had some indirect effect on the rate of increase of lithium sputtering after the onset of nonlinear erosion. In this case, some D may be diffusing into the bulk as the temperature is increased during ion bombardment. This effect necessitates further investigation.

#### **ACKNOWLEDGMENTS**

The authors thank Dr. Jeffrey N. Brooks and Dr. Ahmed Hassanein for insightful discussions. The skillful work of Matthew Hendricks is also acknowledged. This work was supported by the

DOE-ALPS program under grant DEFG02-99-ER54515 and by DOE under contract **DE-AC02-06CH11357**.

## References

- [1] J. N. Brooks, T. D. Rognlien, D. N. Ruzic, and J. P. Allain, *Journal of Nuclear Materials* **290-293**, 185 (2001).
- [2] R.F. Mattas, J.N. Brooks, J.P. Allain, R. Bastasz et al., Presented at the IAEA/TCM on Divertor Concepts (2001).
- [3] R.F. Mattas and et al., *Fusion Engineering Design* **49-50**, 127 (2000).
- [4] J.P. Allain, M. Nieto, M.D. Coventry, R. Stubbers et al., *Fusion Engineering and Design* **72**, 93 (2004).
- [5] J.N. Brooks, J.P. Allain, R. Bastasz, R.P. Doerner et al., *Fusion Science and Technology* **47** (3), 669 (2004).
- [6] A. Hassanein, J.P. Allain, Z. Insepov, and I. Konkashbaev, *Fusion Science and Technology* **47** (3), 686 (2004).
- [7] R. P. Doerner, M.J. Baldwin, R.W. Conn, A.A. Grossman et al., *Journal of Nuclear Materials* **290-293**, 166 (2001).
- [8] R.P. Doerner, M.J. Baldwin, S.I. Krasheninnikov, and D.G. Whyte, *Journal of Nuclear Materials* **313-316**, 385 (2003).
- [9] R.P. Doerner, S.I. Krasheninnikov, and K. Schmid, *Journal of Applied Physics* **95** (8), 4471 (2004).
- [10] J. P. Allain, D. N. Ruzic, and M. R. Hendricks, *Journal of Nuclear Materials* **290-293**, 180 (2001).

- [11] R. Bastasz and J.A. Whaley, *Fusion Engineering and Design* **72**, 111 (2004).
- [12] P. Sigmund, *Physical Review* **184** (2), 383 (1969).
- [13] M.W. Thompson, *Vacuum* **66**, 99 (2002).
- [14] M. W. Thompson, *Philosophical Magazine* **18**, 377 (1968).
- [15] D. A. Thompson, *Journal of Applied Physics* **52** (2), 982 (1981).
- [16] D. A. Thompson, *Radiation Effects* **56**, 105 (1981).
- [17] D. A. Thompson and S. S. Johar, *Applied Physics Letters* **34** (5), 342 (1979).
- [18] C. Claussen, *Nuclear Instruments & Methods in Physics Research* **194**, 567 (1982).
- [19] P. Sigmund, *Applied Physics Letters* **25** (3), 169 (1974).
- [20] P. Sigmund, *Sputtering processes: collision cascades and spikes*. (Academic Press, New York, 1977).
- [21] J.P. Allain, M.D. Coventry, and D.N. Ruzic, *Journal of Nuclear Materials* **313-316**, 645 (2003).
- [22] J.A. Brinkman, *Journal of Applied Physics* **25**, 961 (1954).
- [23] J.A. Brinkman, *American Journal of Physics* **24**, 246 (1956).
- [24] R. Kelly and E. Giani, *Nuclear Instruments & Methods in Physics Research* **209-210**, 531 (1983).
- [25] R. Kelly and A. Miotello, *Nuclear Instruments and Methods in Physics Research B* **141**, 49 (1998).
- [26] R. Kelly, *Radiation Effects* **32**, 91 (1977).
- [27] R. Kelly, *Surface Science* **90**, 280 (1979).
- [28] G. H. Vineyard, *Radiation Effects* **29**, 245 (1976).
- [29] M. M. Jakas, *Radiation Effects and Defects in Solids* **152** (2), 157 (2000).

- [30] R. E. Johnson and R. Evatt, *Radiation Effects* **52**, 187 (1980).
- [31] T. Diaz de la Rubia, R. S. Averback, R. Benedek, and W. E. King, *Physical Review Letters* **59**, 1930 (1987).
- [32] G. S. Chen, *Nuclear Instruments & Methods in Physics Research Section B-Beam Interactions with Materials and Atoms* **71** (1), 7 (1992).
- [33] H.H. Andersen, *Matematisk-fysiske Meddelelser Det Kongelige Danske Videnskabernes Selskab* **43**, 127 (1993).
- [34] H. H. Andersen and H. L. Bay, *Radiation Effects* **19**, 139 (1973).
- [35] R. Kelly, *Nuclear Instruments and Methods in Physics Research B* **46**, 441 (1990).
- [36] E. M. Bringa and R. E. Johnson, *Nuclear Instruments & Methods in Physics Research Section B-Beam Interactions with Materials and Atoms* **143** (4), 513 (1998).
- [37] E. M. Bringa, M. Jakas, and R. E. Johnson, *Nuclear Instruments and Methods in Physics Research B* **164-165**, 762 (2000).
- [38] E. M. Bringa, R. E. Johnson, and L. Dutkiewicz, *Nuclear Instruments and Methods in Physics Research B* **152**, 267 (1999).
- [39] S.S. Johar and D. A. Thompson, *Surface Science* **90**, 319 (1979).
- [40] M. W. Thompson, *Physical Reports* **69** (4), 335 (1981).
- [41] P. Sigmund and M. Szymonski, *Applied Physics A: Solids and Surfaces* **33**, 141 (1984).
- [42] M. Urbassek and P. Sigmund, *Applied Physics A, Solid and Surfaces* **35**, 19 (1984).
- [43] R. S. Averback, *Journal of Nuclear Materials* **216**, 49 (1994).
- [44] P. Sigmund and C. Claussen, *Journal of Applied Physics* **52** (2), 990 (1981).
- [45] R.E. Johnson, *Reviews of Modern Physics* **68**, 305 (1996).
- [46] R. S. Nelson, 343 (1963).

- [47] R. S. Nelson, *Philosophical Magazine* **11**, 291 (1965).
- [48] K. Besocke, S. Berger, W. O. Hofer, and U. Littmark, *Radiation Effects* **66**, 35 (1982).
- [49] R. Behrisch and W. Eckstein, *Nuclear Instruments and Methods in Physics Research B* **82**, 255 (1993).
- [50] M.F. Dumke, T. A. Tombrello, R. A. Weller, R.M. Housley et al., *Surface Science* **124**, 407 (1983).
- [51] M. H. Shapiro, K. R. Bengtson, and T. A. Tombrello, *Nuclear Instruments and Methods in Physics Research B* **103**, 123 (1995).
- [52] K. M. Hubbard, R. A. Weller, D. L. Weathers, and T. A. Tombrello, *Nuclear Instruments and Methods in Physics Research B* **40**, 278 (1989).
- [53] K. M. Hubbard, R. A. Weller, D. L. Weathers, and T. A. Tombrello, *Nuclear Instruments and Methods in Physics Research B* **36**, 395 (1989).
- [54] H. H. Andersen and H. L. Bay, *Journal of Applied Physics* **45** (2), 953 (1974).
- [55] Mai Ghaly, R.S. Averback, and T. Diaz de la Rubia, *Nuclear Instruments and Methods in Physics Research B* **102**, 51 (1995).
- [56] R.S. Averback and Mai Ghaly, *Nuclear Instruments and Methods in Physics Research B* **127-128**, 1 (1997).
- [57] H.H. Andersen, A. Brunelle, S. Della-Negra, J. Depauw et al., *Physical Review Letters* **80** (24), 5433 (1998).
- [58] M.H. Shapiro and T.A. Tombrello, *Nuclear Instruments and Methods in Physics Research B* **152**, 221 (1999).
- [59] M.H. Shapiro and T.A. Tombrello, *Surface Science* **453**, 143 (2000).

- [60] E.P. Vaulin, N.E. Georgieva, T.P. Martynenko, and L.V. Feoktistov, *Soviet Journal of Plasma Physics* **7** (2), 239 (1981).
- [61] Lukasz Dutkiewicz, Roman Pedrys, and Jørgen Schou, *Nuclear Instruments and Methods in Physics Research B* **115**, 478 (1996).
- [62] M. Szymonski and A. de Vries, *Radiation Effects* **54**, 135 (1981).
- [63] J. P. Allain, D. N. Ruzic, and M. R. Hendricks, *Journal of Nuclear Materials* **290-293**, 33 (2001).
- [64] J.P. Allain, Ph.D., University of Illinois at Urbana-Champaign, 2001.
- [65] M.D. Coventry, J.P. Allain, and D.N. Ruzic, *Journal of Nuclear Materials* **313-316**, 640 (2003).
- [66] J.P. Allain and D.N. Ruzic, *Nuclear Fusion* **42**, 202 (2002).
- [67] J.P. Allain and D.N. Ruzic, in *NATO Science Series: Hydrogen and Helium Recycling at Plasma Facing Materials*, edited by A. Hassanein (Kluwer Academic Publishers, Dordrecht, 2002), Vol. 54, pp. 73.
- [68] J.P. Allain, D.N. Ruzic, D.A. Alman, and M.D. Coventry, *Nuclear Instruments and Methods in Physics Research B* **239**, 347 (2005).
- [69] D. N. Ruzic, *Nuclear Instruments and Methods in Physics Research* **B47**, 118 (1990).
- [70] R. Bastasz and W. Eckstein, *Journal of Nuclear Materials* **290-293**, 19 (2001).
- [71] A. R. Krauss and D. M. Gruen, *Journal of Nuclear Materials* **85 & 86**, 1179 (1979).
- [72] J.P. Allain, J.N. Brooks, D.A. Alman, and L.E. Gonzalez, *Journal of Nuclear Materials* **337-339**, 94 (2005).
- [73] M.M. Jakas and D.E. Harrison Jr., *Physical Review Letters* **55** (17), 1782 (1985).
- [74] P. Sigmund, *Sputtering by Particle Bombardment I*. (Springer-Verlag, Berlin, 1981).

- [75] C. Garcia-Rosales, W. Eckstein, and J. Roth, *Journal of Nuclear Materials* **218**, 8 (1994).
- [76] Y. Yamamura, Y. Itikawa, and N. Itoh, IPPJ-AM-26 (Institute of Plasma Physics, Nagoya, Japan) (1983).
- [77] M.W. Thompson, *Nuclear Instruments & Methods in Physics Research* **B18**, 411 (1987).
- [78] S.V. Mirnov, E.A. Azizov, V.A. Evtikhin, V.B. Lazarev et al., *Plasma Physics and Controlled Fusion* **48**, 821 (2006).
- [79] M.L. Yu, in *Sputtering by Particle Bombardment III*, edited by R. Behrisch and K. Wittmaack (Springer-Verlag, Berlin, 1991), Vol. 64.
- [80] R. Brako and D.M. Newns, *Surface Science* **108**, 253 (1981).
- [81] C.C. Addison, *The Chemistry of the Liquid Alkali Metals*. (John Wiley & Sons Ltd., New York, 1984).
- [82] M.J. Baldwin, R.P. Doerner, S.C. Luckhardt, and R.W. Conn, *Nuclear Fusion* **42**, 1318 (2002).

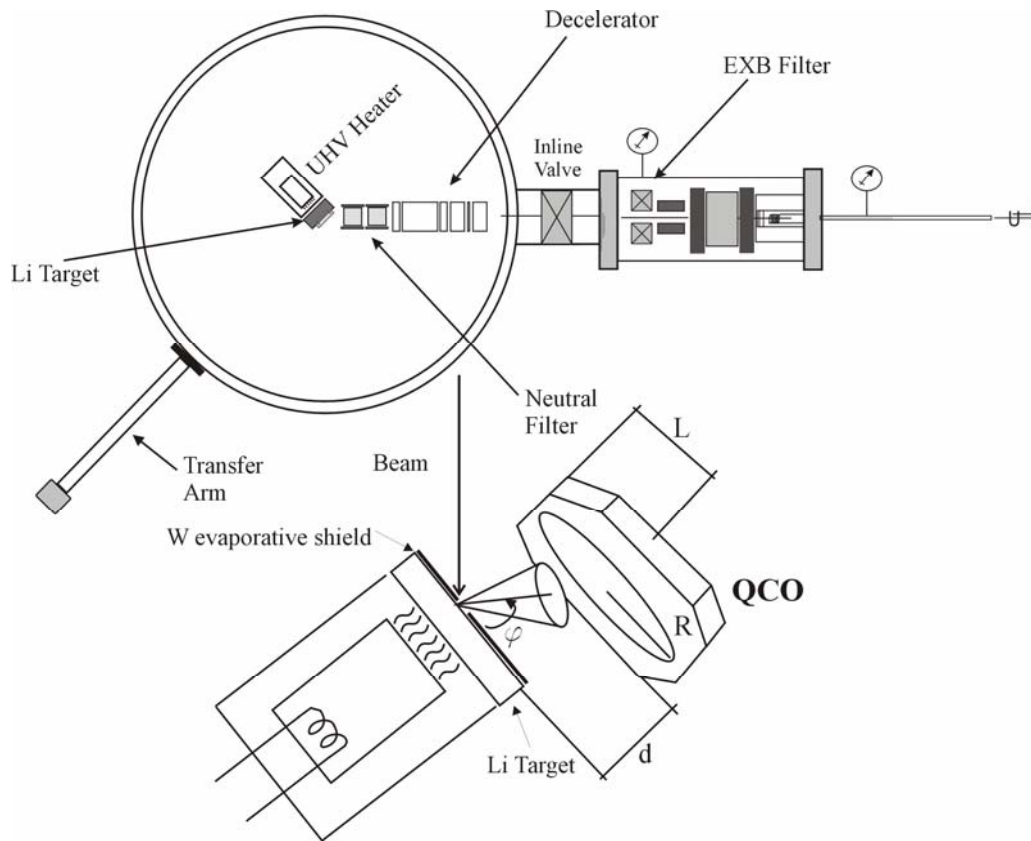


Figure 1. The Ion-surface InterAction Experiment (IIAX). The experimental device is shown with two differentially pumped chambers: on the right the ion gun chamber, and on the left the main chamber where the lithium target sample is located. The inset diagram shows the position of the QCO with respect to the lithium target. The distance between the lithium target and the QCO is  $d$ , the angle of ejected flux  $\phi$ , the radius of the crystal,  $R$  and the length from the edge of QCM to center of crystal is designated  $L$ .

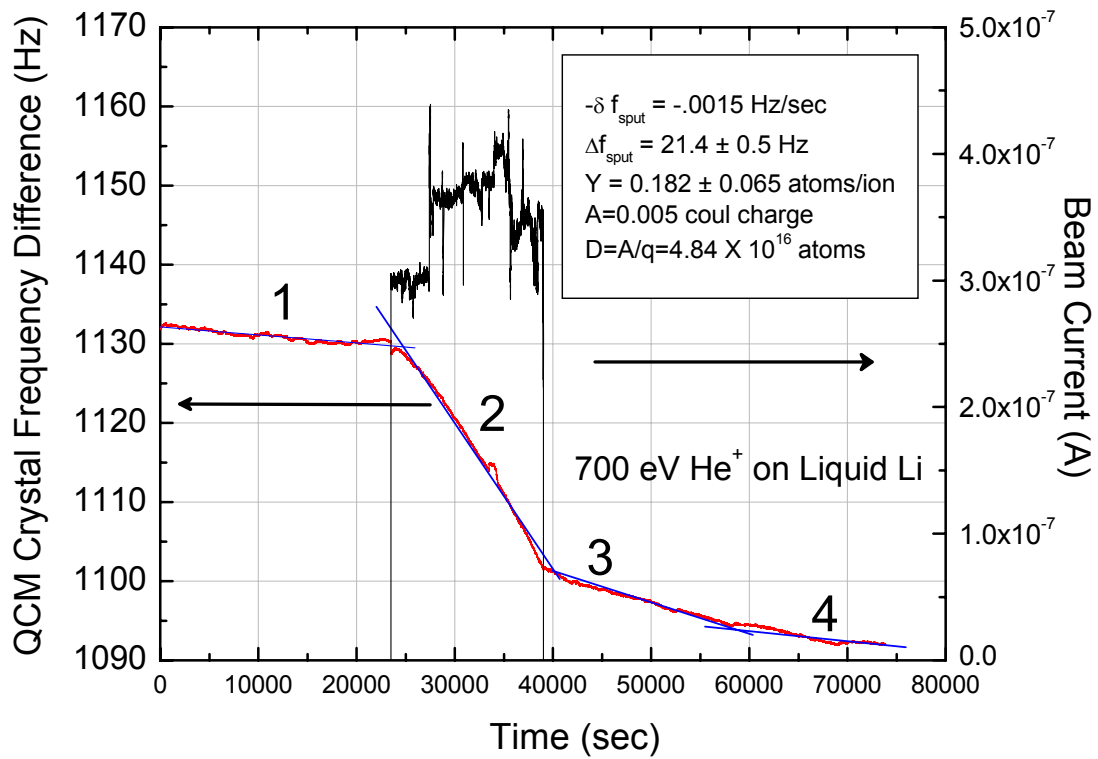


Figure 2. The data show a decrease in the crystal frequency as evaporated lithium is collected. As the liquid sample is exposed to the ion beam, the QCM crystal measures both sputtering and evaporation fluxes.

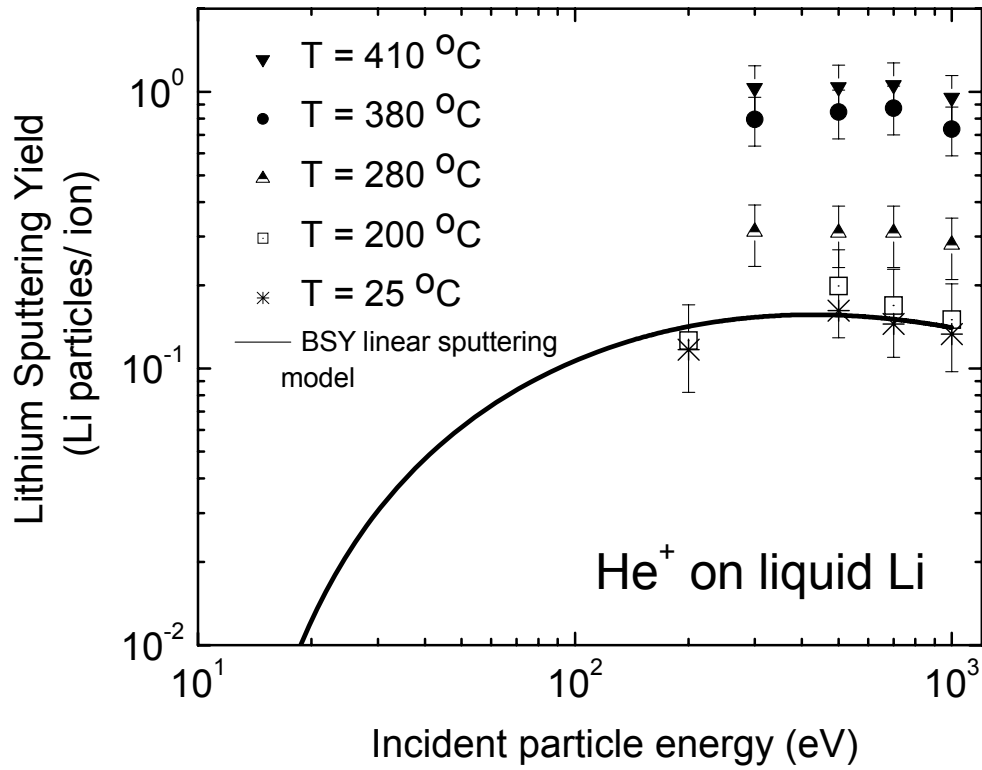


Figure 3. Measurements of the sputtering yield of lithium bombarded by He<sup>+</sup> ions at 45-degree incidence for a variety of incident particle energies and target temperatures. The data is plotted with the BSY model based on linear sputtering theory. At each incident particle energy the nonlinear behavior of the lithium-sputtering yield is shown as the temperature increases.

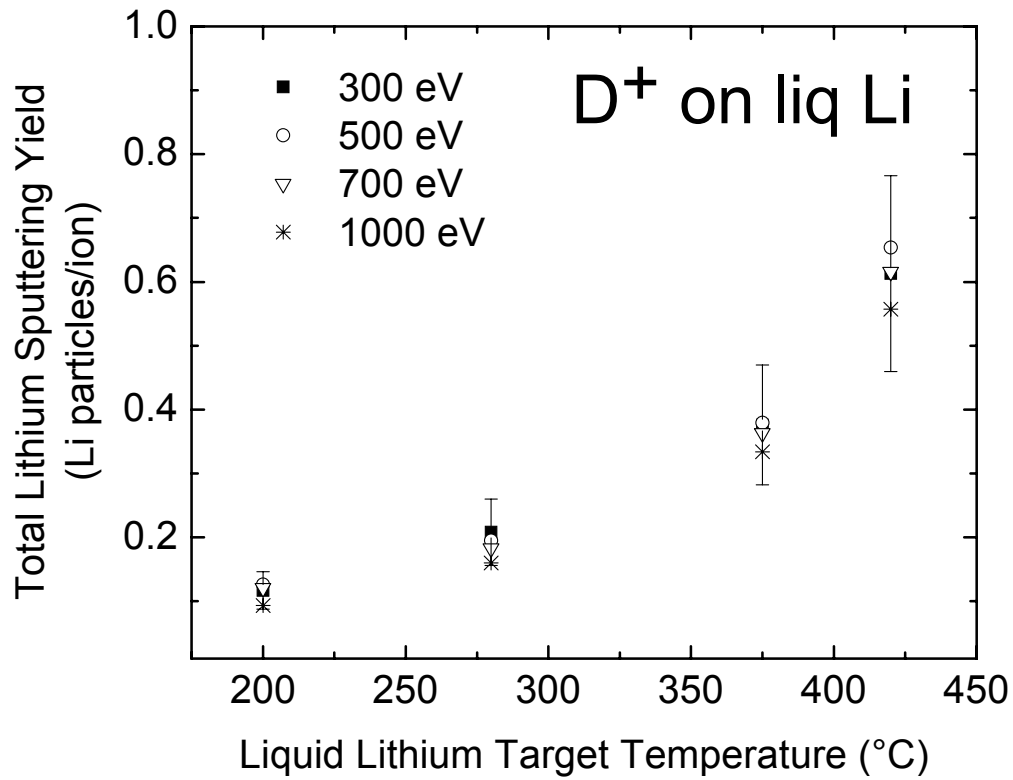


Figure 4. Measurements of temperature-dependent lithium sputtering from D<sup>+</sup> bombardment for various incident particle energies at 45-degree incidence of liquid lithium.

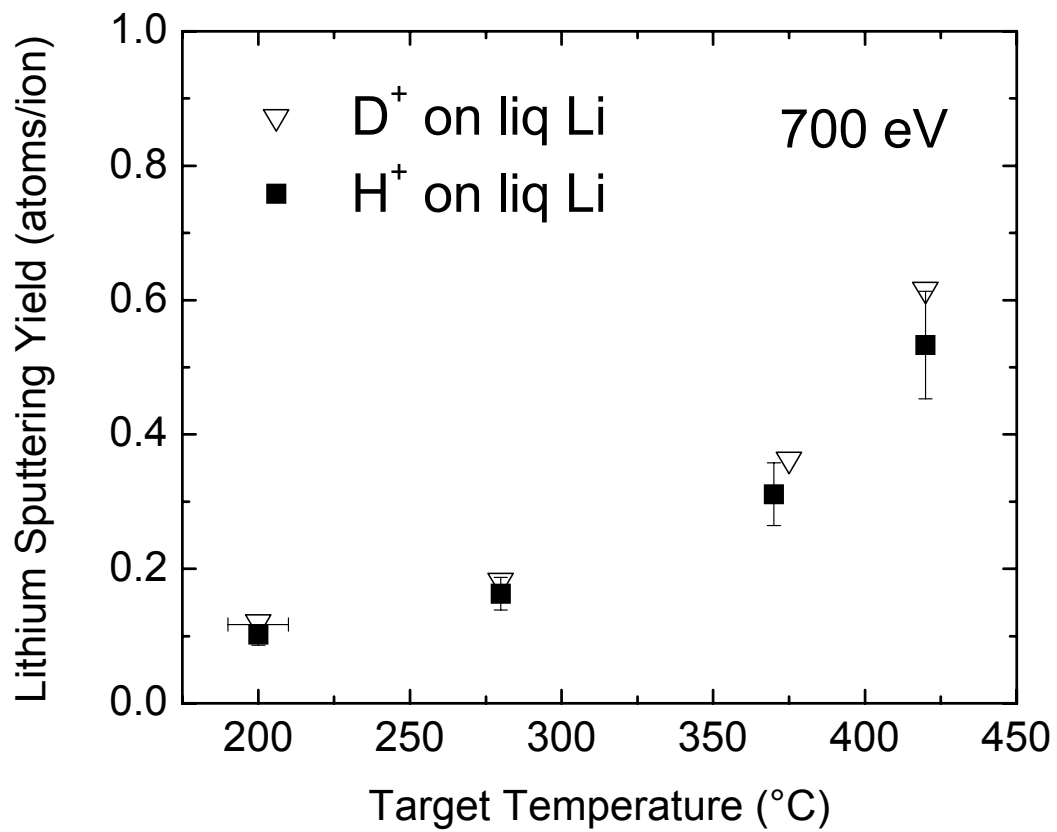


Figure 5. Lithium-sputtering yield from singly-charged deuterium and hydrogen ions on liquid lithium at 700 eV and oblique incidence as a function of target temperature.

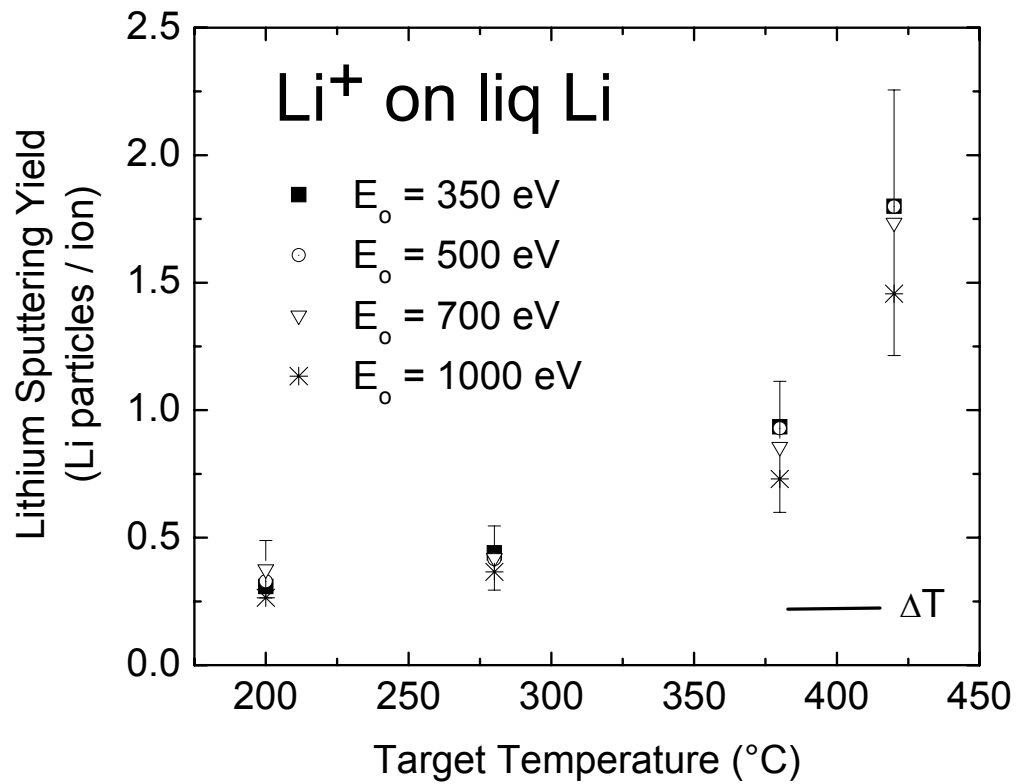


Figure 6. Measurements of temperature-dependent lithium sputtering from  $\text{Li}^+$  bombardment for various incident particle energies at 45-degree incidence of liquid lithium.

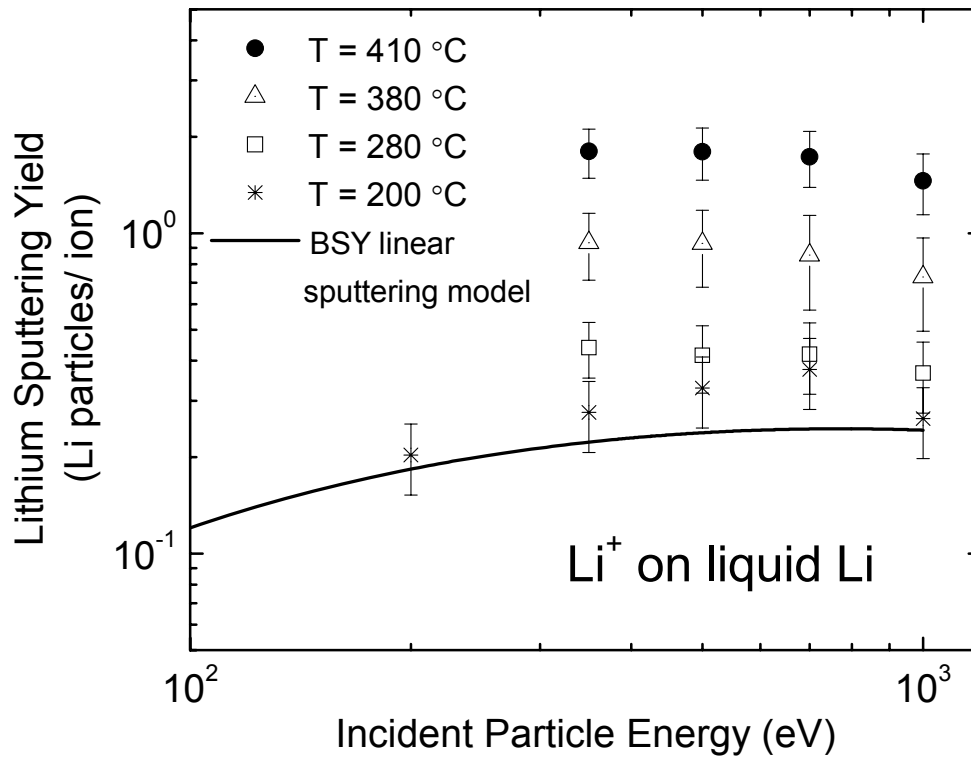


Figure 7. Measurements of lithium self-sputtering yield as a function of incident particle energy for various temperatures at 45-degree incidence. Also plotted is the BSY linear sputtering yield model for comparison.

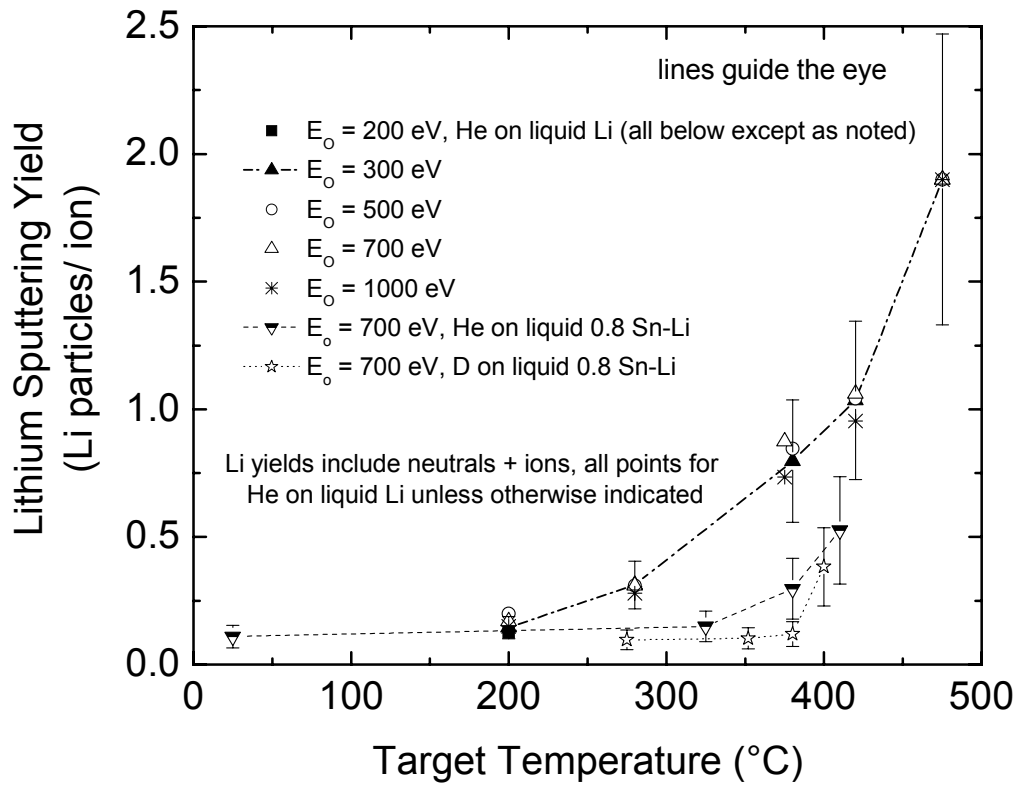


Figure 8. Lithium sputtering yield from  $\text{He}^+$  bombardment on liquid lithium for various incident particle energies and temperatures at oblique incidence. Also shown is the lithium sputtering yield from tin-lithium surfaces from both  $\text{He}^+$  and  $\text{D}^+$  bombardment.

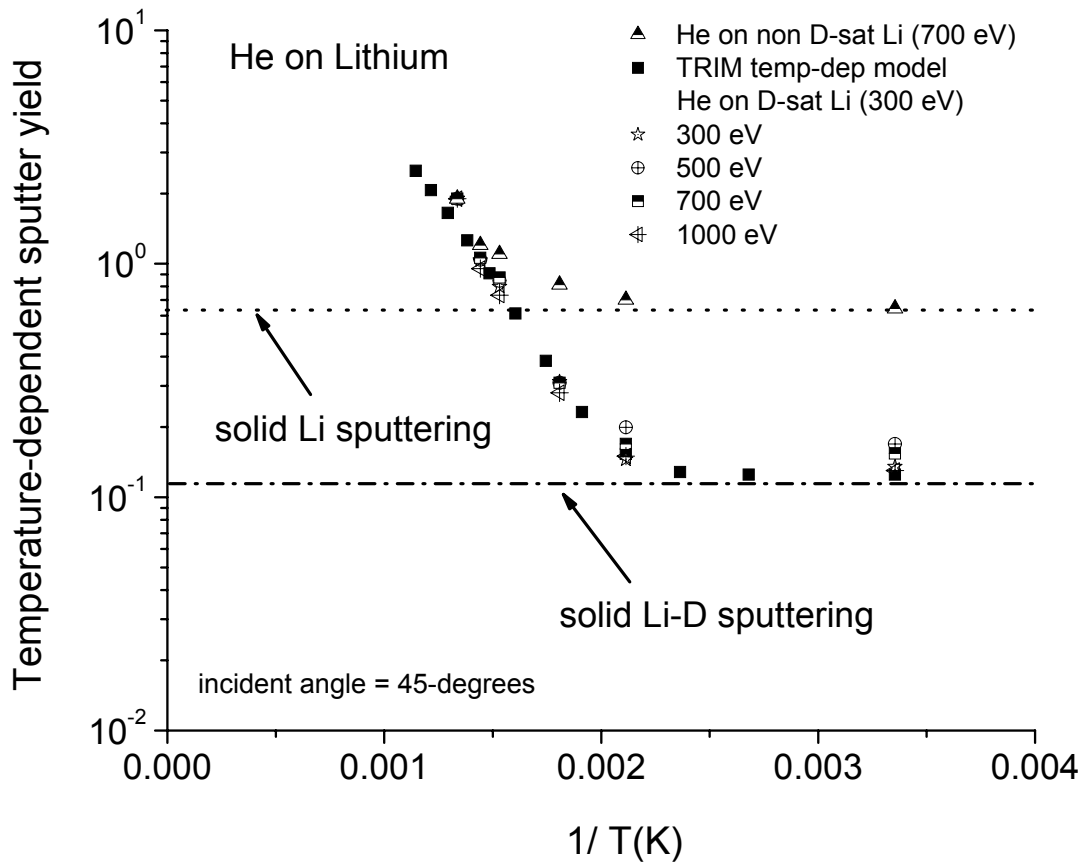


Figure 9. Inverse-temperature dependence of the lithium sputter yield parametrized with incident particle energy and compared to a TRIM temperature-dependent model [21].

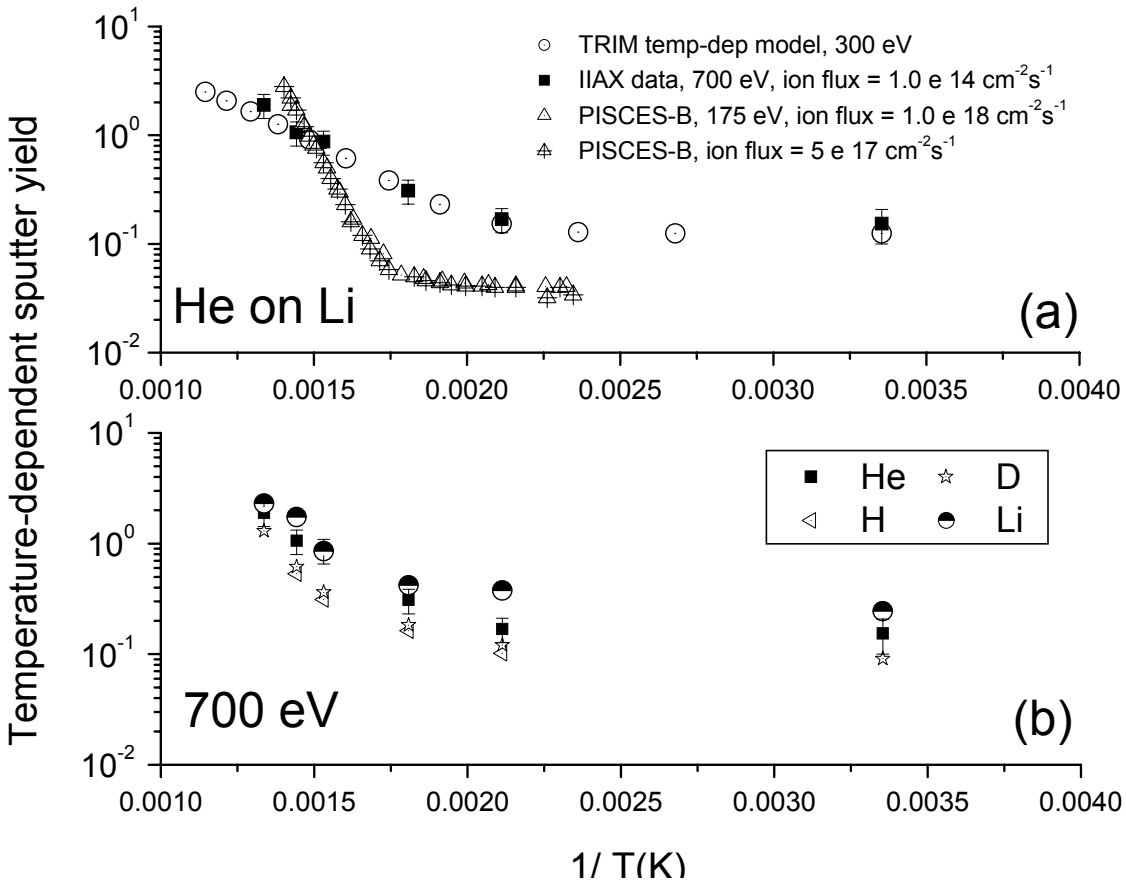


Figure 10. Inverse-temperature dependence of the lithium sputter yield parametrized with (a) incident particle energy compared to a TRIM temperature-dependent model [21] and incident flux, and (b) incident mass.

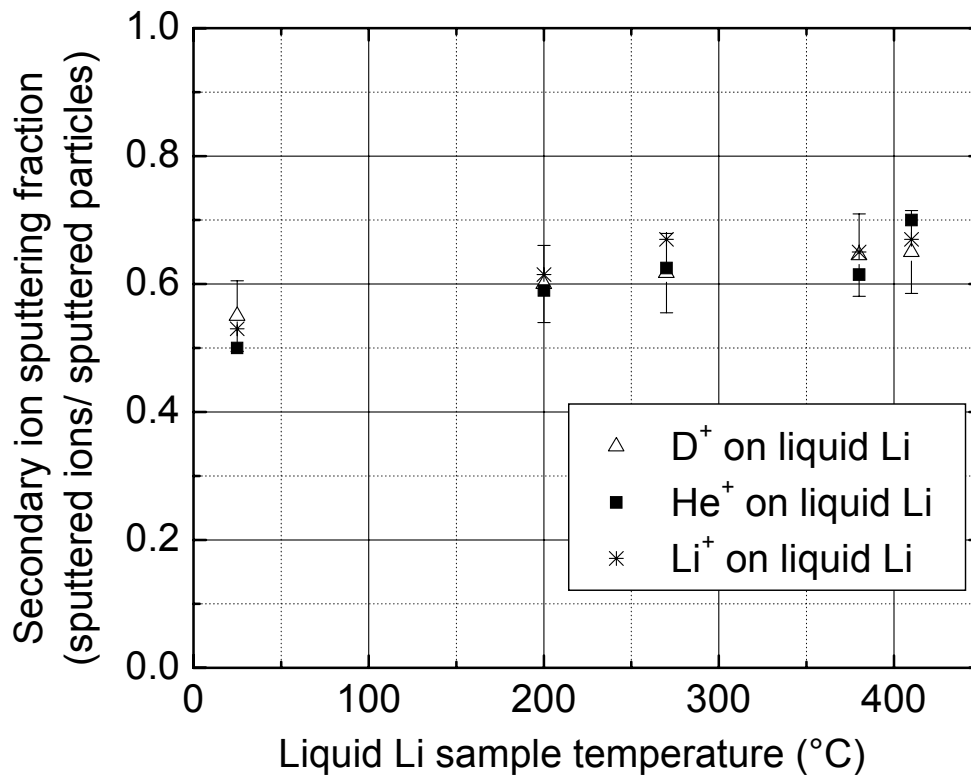


Figure 11. Measurements of the ion-induced secondary ion sputtering fraction as a function of temperature for 700 eV  $D^+$ ,  $He^+$ , and  $Li^+$  bombardment at 45-degree incidence on lithium.

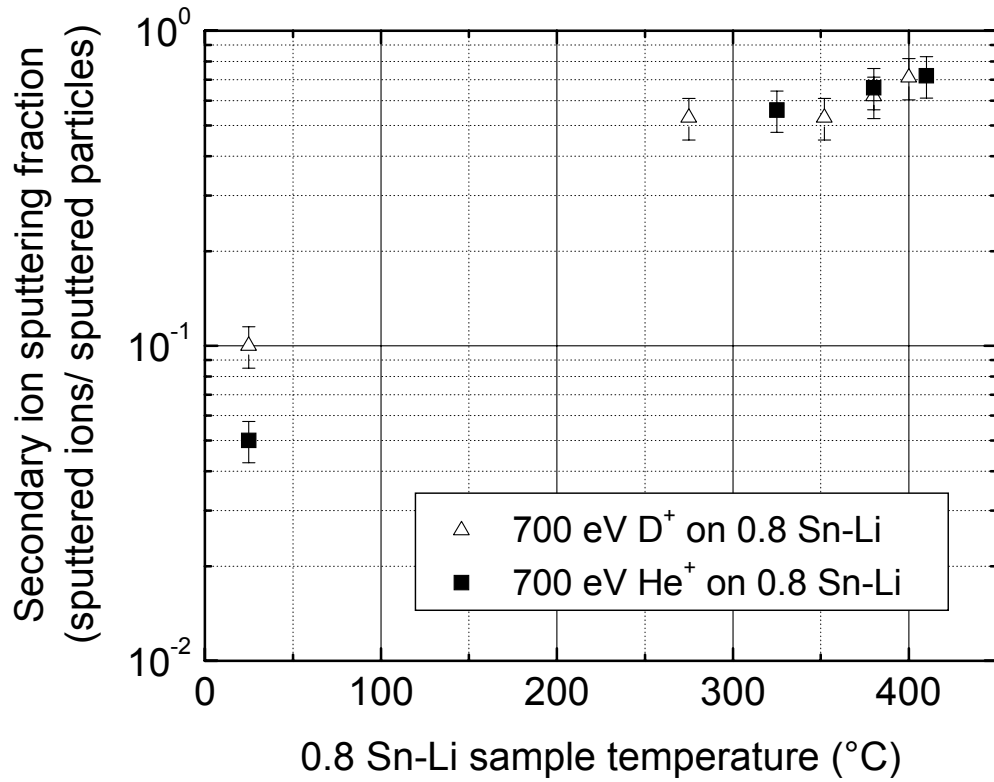


Figure 12. Measurements of the ion-induced secondary ion sputtering fraction as a function of temperature for 700 eV D<sup>+</sup> and He<sup>+</sup> bombardment at 45-degree incidence on 0.8 Sn-Li.

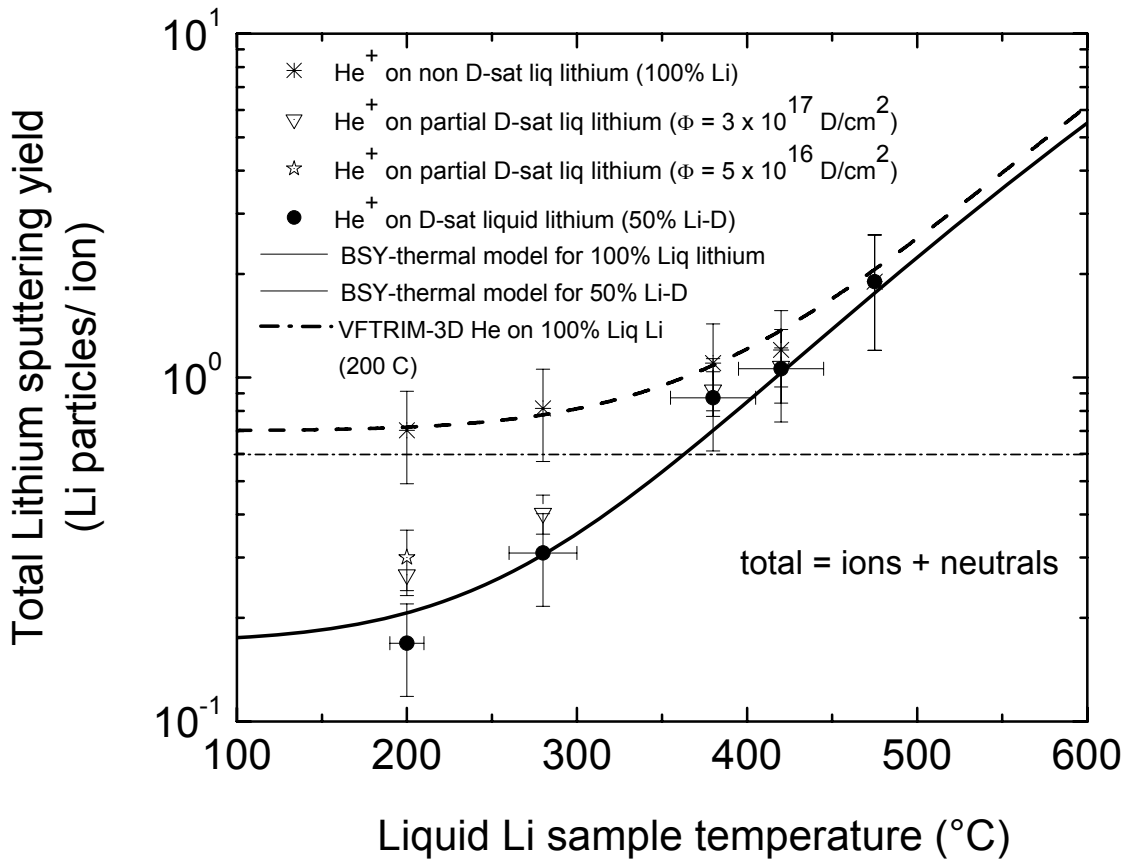


Figure 13. Lithium sputtering yield as function of sample temperature and deuterium fluence exposure. Also plotted is the BSY-thermal model for deuterium-treated and non deuterium-treated lithium surfaces.

The submitted manuscript has been created by UChicago Argonne, LLC, Operator of Argonne National Laboratory ("Argonne"). Argonne, a U.S. Department of Energy Office of Science laboratory, is operated under Contract No. DE-AC02-06CH11357. The U.S. Government retains for itself, and others acting on its behalf, a paid-up nonexclusive, irrevocable worldwide license in said article to reproduce, prepare derivative works, distribute copies to the public, and perform publicly and display publicly, by or on behalf of the Government.